Imperial College London

Department of Earth Science and Engineering

MSc in Applied Computational Science and Engineering

Independent Research Project

Project Plan

Physics-Constrained Koopman Modeling under Sparse Observations

by

Wenxuan Yuan

Email: wenxuan.yuan24@imperial.ac.uk

GitHub username: esemsc-wy524

Repository: https://github.com/ese-ada-lovelace-2024/irp-wy524

Supervisors:

Prof. Sibo Cheng
Dr. Rossella Arcucci

June 2025

AI Acknowledgement Statement

In the process of carrying out the Independent Research Project, I used the following generative AI tool:

Anthropic Claude Sonnet 4, Claude Opus 4 (https://claude.ai/)

OpenAI ChatGPT-4o (https://chatgpt.com/)

- **Purpose**: Used for developing the preliminary experimental framework, information gathering, and technical discussion
- **Specific applications**:
  - Assisted in coding the initial experimental framework for the 1D heat equation.
  - Searched for technical information and reference materials about Koopman operator theory, variational inference, optimal transport method, etc.
  - Assisted with debugging and optimizing of experimental code

Important clarification: No generative AI tools were used in the writing, drafting, editing, or content generation of this written project plan. All written content, methodology design, and theoretical framework represent my own original thinking and expression. The core contributions (including model assumptions and combining variational inference with optimal transport constraints in RKHS) are entirely my own conceptual developments.

Declaration: While generative AI tools assisted with code development and information gathering, all ideas, methodological innovations, and written content are my own original thoughts. I have signed the Academic Integrity Declaration confirming compliance with all relevant academic integrity policies.

Abstract

Reconstructing high-fidelity physical states from sparse sensor observations is a fundamental challenge in modelling complex dynamical systems. Due to the sparsity of data availability, data-driven methods have limited performance, while methods based on physics are computationally expensive and hard to generalize. This project proposes a novel framework integrating physical constraints into Koopman dynamics modelling under sparse observation conditions.

The methodology establishes a mapping hypothesis framework: (1) nonlinear encoding from sparse observations to Koopman latent space, (2) linear dynamics evolution, and (3) physics-constrained decoding to physical space. Key innovations include using variational inference in Reproducing Kernel Hilbert Space (RKHS) to construct physics-embedded mappings and applying optimal transport theory to guide constraint handling.

Preliminary validation (retaining the core idea and using a simple model) indicates that in 1D heat conduction problems, the Koopman model parameterized by neural networks can learn linear dynamical structures. And the physical regularization terms apply to some extent help the hidden space learn some certain cluster structure. During the implementation of this project, a step by step experimental validation method is adopted.

1 Introduction

Reconstructing high-fidelity flow fields from sparse sensor observations is a key challenge in modeling complex dynamic systems in science and engineering [21]. In practical applications, due to cost, technical or environmental limitations, we can often only obtain partial observation data of the system. The sparsity makes it challenging to do accurate system state estimation and prediction. Traditional data-driven methods [13] have limited performance when the available data is insufficient. In contrast, physics-based numerical approaches [1, 7], are built on solid theory, but they often require heavy computation and are hard to apply directly to complex real-world systems. With the rapid development of deep learning technology, using neural networks to recover the real physical state from sparse observations [4, 5, 8, 9] has gradually become a research trend in recent years.

Koopman operator theory [3] is a high-dimensional linear modeling framework for nonlinear dynamic systems, and realizes linear evolution description by embedding nonlinear systems into a high-dimensional observable function space. This theory shows great potential in fluid dynamics [16], climate modeling [18], biological systems[2] and other fields. In recent years, more and more research works [10, 17, 23] have integrated Koopman theory with deep learning, learning the Koopman invariant subspace of the system while maintaining linear evolution characteristics to improve the flexibility and accuracy of modeling.

However, the inherent black-box nature of neural networks [6] exposes limitations under sparse observation conditions. Existing physical information embedding methods can be divided into two categories: one is to add physical constraints as regularization terms to the loss function. Although this soft constraint method is simple to implement [11, 14, 20], the neural network itself is still a black box model. It is hard for us to explain the specific influence of adding physical regularization terms on model behavior strictly and no way to guarantee the strict satisfaction of physical constraints; the other is to directly embed physical laws into the network structure through hard constraints [22], but these methods face the problem of underdetermination under sparse observation conditions, which may lead to non-unique solutions and numerical instability. In addition, most existing methods ignore the linear structural characteristics of the Koopman operator itself and fail to fully utilize its advantages in processing sparse data.

To address the above challenges, this study proposes a new method to effectively embed physical constraints into decoding of Koopman latent variables under sparse observation conditions. Specifically, we construct a mapping hypothesis framework: nonlinear encoding from sparse observation space to Koopman linear latent space, linear dynamics evolution in the latent space, and physical constraint embedding decoding from the latent space to the physical space. The innovations of this method are: (1) using the variational inference [1, 12] framework to construct a physical constraint embedding mapping in the RKHS [15] to guarantee the strict satisfaction of physical laws; (2) Using the optimal transport theory [19] to handle constraint violations, providing a principled constraint handling method.

Since this is a relatively new research direction, this project will adopt a progressive experimental verification strategy. We will start from simple low-dimensional data and gradually extend to complex actual physical systems to systematically verify the feasibility and effectiveness of the methodology. If time permits, we will conduct a comprehensive comparative analysis with state-of-art methods to evaluate the advantages of the proposed method in terms of prediction accuracy, physical consistency, and computational efficiency.

2 Methodology

2.1 Model Assumptions and Framework Design

In this study, we develop a hypothetical mapping framework (Figue 1) for the modeling of dynamical systems under sparse observation conditions. For actual observation data, we assume that there are three related state spaces:

- **Latent space:** z_t — Koopman linear latent space state, representing the intrinsic dynamic information of system.
- **Physical space:** $Y_t = H(z_t)$ — real-world physical space state, satisfying the physical constraint condition $F(H(z_t)) \approx 0$
- **Observation space:** $X_t = G(Y_t) + \epsilon_0$ — sparse observation state variable, where G is the observation function and ϵ_0 is the observation noise

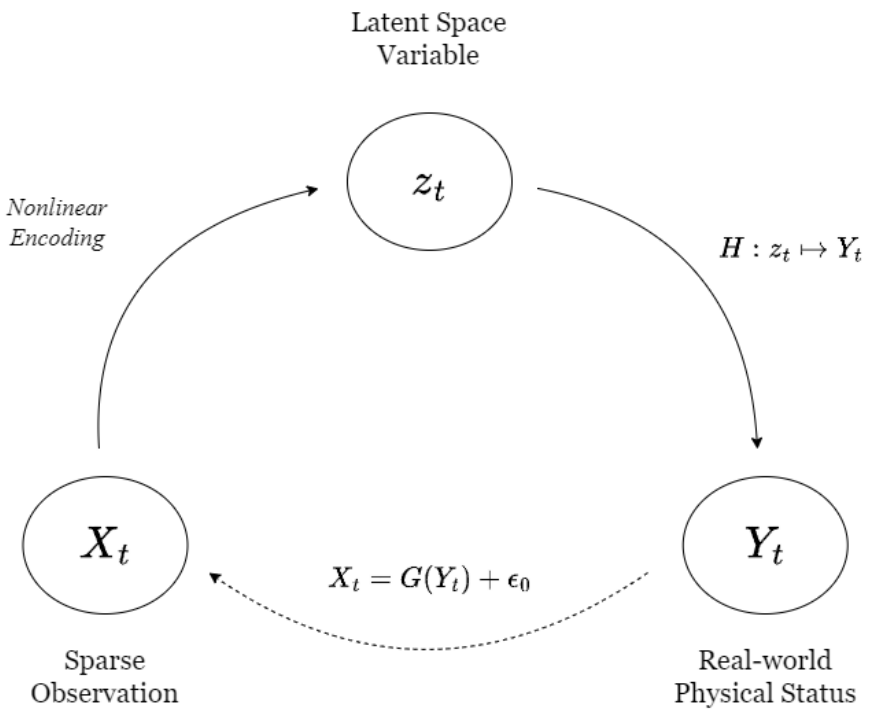

Figure 1: The hypothetical mapping relationship between the three spaces, where the dotted line represents observations in the real world.

Mapping relationships:

Our proposed framework involves the following three core mappings:

1. **Observation to latent space:** $\phi_{NN} : X_{t-N:t} \mapsto z_t$
   Nonlinear encoding from sparse observation to latent space.
2. **Latent space dynamics:** $\phi_K : z_t \mapsto z_{t+1}$
   Linear dynamic evolution in latent space (Koopman operator).

3. **Latent to physical space:** $H : z_t \mapsto Y_t$
   Constrained embedding decoding from latent space to physical space.

2.2 Encoding mapping design

Objective:
Learn the mapping $\phi_{NN} : X_{t-N:t} \mapsto z_t$ from sparse observations to latent space, so that the latent space state z_t contains sufficient information to predict the physical state Y_t.

Information Preservation Strategy:
we employ *variational information maximization* to preserve sufficient predictive information in the latent representation. Specifically, we optimize the mutual information between the latent variable z and the physical state Y:

$$\max_{\phi_{NN}} I(z;Y) = \mathbb{E}_{p(z,y)}[\log q_\phi(z|y)] - \mathbb{E}_{p(z)}[\log q_\phi(z)]$$

2.3 Dynamic evolution modeling

Objective:
Model the latent space evolution $\phi_K : z_t \mapsto z_{t+1}$ as a linear dynamical process, in alignment with the Koopman operator framework. we propose two implementation schemes:

Solution 1: Theoretical Construction via Conditional Mean Embedding (CME)
This approach builds the Koopman operator explicitly based on the theory of Conditional Mean Embedding:

$$z_{t+1} = \mathbb{E}[z_{t+1} \mid z_t] = C_{z_{t+1}z_t} C_{z_t z_t}^{-1}$$

where $C_{z_{t+1}z_t}, C_{z_t z_t}^{-1}$ are covariance operators in a Reproducing Kernel Hilbert Space (RKHS).

Solution 2: Soft-Constrained Neural Network
Alternatively, we implement ϕ_K as a trainable neural network while encouraging linearity via:

$$\mathcal{L}_{\text{linearity}} = \|z_{t+1} - \phi_K(z_t)\|^2$$

2.4 Physical Constraint Embedding Mapping

Core Challenge:
Design a mapping $H : z_t \mapsto Y_t$ that satisfies:

- **Physical consistency:** $F(H(z)) \approx 0$
- **Prediction accuracy:** $\|Y_t - H(z_t)\|^2$ minimized
- **Interpretability:** Reflect physical variables and boundary conditions

Baseline Method: Residual Physical Loss (PINN-style)
Use a method similar to PINN to directly add physical constraints to the loss function:

$$\mathcal{L}_{\text{PINN-style}} = \|Y_t - H_\theta(z_t)\|^2 + \lambda_{\text{phy}}\|F(H_\theta(z_t))\|^2$$

Proposed Method: Variational Embedding with Optimal Transport Constraints
We propose to construct a physical constraint embedding mapping in the reproducing kernel Hilbert space (RKHS), including:

1. **Variational framework:**
   Treat H as a function drawn from a Gaussian Process (GP), and impose a physics-informed prior over its output:
   $$p(H) \propto \exp(-\lambda_{\text{phy}}\|F(H(z))\|^2)$$
2. **Optimal transport constraints:**
   Use Wasserstein distance W_2 to measure the discrepancy between predicted physical states and a target physics-aligned distribution:
   $$\mathcal{L}_{\text{physics}} = W_2\left(q_\phi(H(z)),\ p_{\text{phy}}(Y)\right)$$
   This provides a principled and geometry-aware way to impose soft constraints.
3. **Joint variational optimization:**
   Optimize the evidence lower bound (ELBO) jointly with constraint penalties:

$$\mathcal{L}_{\text{total}} = \underbrace{\mathcal{L}_{\text{reconstruction}}}_{\text{Prediction fidelity}} + \alpha \underbrace{\mathcal{L}_{\text{physics}}}_{\text{Constraint satisfaction}} + \beta \underbrace{\mathcal{L}_{\text{info}}}_{\text{Information preservation}} + \gamma \underbrace{\mathcal{L}_{\text{koopman}}}_{\text{Dynamic consistency}}$$

For more detailed mathematical process, please refer to Appendix A

3 Key Challenges and Potential Problems

Although the proposed method is innovative in theory, there are still some key challenges in the implementation process, which need to be focused on and resolved during the project.

3.1 Theoretical Feasibility

Balancing theory and flexibility in Koopman modeling. Both Koopman operator implementations come with trade-offs. The CME-based approach strictly enforces linearity and interpretability but lacks adaptability to data. In contrast, neural network-based methods are more flexible but risk deviating from Koopman's theoretical foundation. Striking a practical balance between theoretical rigor and empirical performance remains a core challenge.

Strong coupling between modules. The mappings ϕ_{NN}, ϕ_K, and H are highly interdependent. For instance, the performance of H depends on the latent representations learned by ϕ_{NN}. This interdependence can lead to error propagation and makes the joint optimization process more sensitive and fragile.

3.2 Computational complexity

Heavy nested optimization structure. The full model pipeline involves several computationally intensive components: end-to-end neural training, Gaussian process inference with $O(N^3)$ complexity, and iterative Sinkhorn solvers. While this structure allows expressive modeling, it can be prohibitively expensive for high-dimensional or large-scale systems.

Scalability bottlenecks. As system size grows, both the covariance matrices in variational inference and cost matrices in optimal transport increase rapidly, potentially limiting applicability to real-world large-scale problems.

3.3 Training strategy stability

Lack of convergence guarantee for staged training. While staged training can help reduce interference between modules, it lacks a theoretical guarantee of convergence to a global optimum. Conflicts between physics constraints and data-fitting objectives may lead the model into suboptimal local minima.

3.4 Verification and evaluation challenges

Evaluating physical consistency. Although Wasserstein distance provides a rigorous way to measure constraint violation, its intuitive physical meaning remains to be verified. Developing more intuitive and reliable indicators for assessing physical consistency is still an open question.

Generalization under sparse conditions. Under sparse observation conditions, it's hard to evaluate whether the model can generalize to unseen system states or to new sparsity patterns. Ensuring that physical constraints continue to hold under such out-of-distribution settings is crucial for practical deployment.

Preliminary Validation:
To test basic feasibility, a simple experiment was conducted:

- Fixed a linear neural notework to present Koopman operator K;
- Used simple fully connected networks for ϕ_{NN} and H;
- Replaced optimal transport with an L_2 penalty: $\mathcal{L}_{\text{physics}} = \lambda \|F(H(z))\|^2$;
- Tested on a *1D heat conduction system*.

Results and discussion are presented in Appendix B.

4 Project Plan

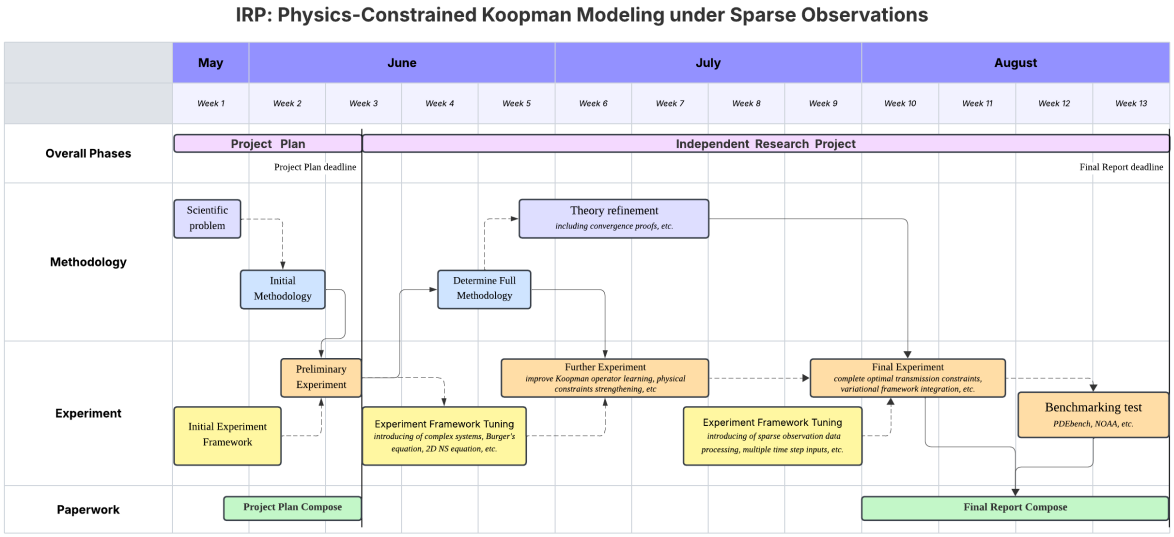

References

[1] R Acar and C R Vogel. Analysis of bounded variation penalty methods for ill-posed problems. *Inverse Problems*, 10(6):1217, dec 1994.

[2] Abdallah Alameddine. Systems biology modeling of cancer nonlinear dynamics. In *Systems Biology*, pages 121–134. Springer, 2023.

[3] Steven L. Brunton, Marko Budišić, Eurika Kaiser, and J. Nathan Kutz. Modern koopman theory for dynamical systems. *SIAM Review*, 64(2):229–340, 2022.

[4] Steven L. Brunton, Joshua L. Proctor, and J. Nathan Kutz. Discovering governing equations from data by sparse identification of nonlinear dynamical systems. *Proceedings of the National Academy of Sciences*, 113(15):3932–3937, April 2016.

[5] Sibo Cheng, Che Liu, Yike Guo, and Rossella Arcucci. Efficient deep data assimilation with sparse observations and time-varying sensors. *Journal of Computational Physics*, 496:112581, January 2024.

[6] Judith E Dayhoff and James M DeLeo. Artificial neural networks: opening the black box. *Cancer: Interdisciplinary International Journal of the American Cancer Society*, 91(S8):1615–1635, 2001.

[7] Richard P Dwight. Bayesian inference for data assimilation using least-squares finite element methods. In *IOP Conference Series: Materials Science and Engineering*, volume 10, page 012224. IOP Publishing, 2010.

[8] Hongwei Fan, Sibo Cheng, Audrey J. De Nazelle, and Rossella Arcucci. ViTAE-SL: A vision transformer-based autoencoder and spatial interpolation learner for field reconstruction. *Computer Physics Communications*, 308:109464, March 2025.

[9] Kai Fukami, Romit Maulik, Nesar Ramachandra, Koji Fukagata, and Kunihiko Taira. Global field reconstruction from sparse sensors with Voronoi tessellation-assisted deep learning. *Nature Machine Intelligence*, 3(11):945–951, October 2021.

[10] Mars Liyao Gao, Jan P. Williams, and J. Nathan Kutz. Sparse identification of nonlinear dynamics and Koopman operators with Shallow Recurrent Decoder Networks, April 2025.

[11] Anran Jiao, Qile Yan, Jhn Harlim, and Lu Lu. Solving forward and inverse PDE problems on unknown manifolds via physics-informed neural operators, July 2024.

[12] Diederik P. Kingma, Tim Salimans, Ben Poole, and Jonathan Ho. Variational Diffusion Models, April 2023.

[13] Jack P.C. Kleijnen. Kriging metamodeling in simulation: A review. *European Journal of Operational Research*, 192(3):707–716, 2009.

[14] Zongyi Li, Hongkai Zheng, Nikola Kovachki, David Jin, Haoxuan Chen, Burigede Liu, Kamyar Azizzadenesheli, and Anima Anandkumar. Physics-Informed Neural Operator for Learning Partial Differential Equations. *ACM / IMS Journal of Data Science*, 1(3):1–27, September 2024.

[15] Jonathan H. Manton and Pierre-Olivier Amblard. A Primer on Reproducing Kernel Hilbert Spaces, November 2015.

[16] Igor Mezić. Analysis of fluid flows via spectral properties of the koopman operator. *Annual review of fluid mechanics*, 45(1):357–378, 2013.

[17] J. Nathan Kutz, J. L. Proctor, and S. L. Brunton. Applied Koopman Theory for Partial Differential Equations and Data-Driven Modeling of Spatio-Temporal Systems. *Complexity*, 2018(1):6010634, 2018.

[18] Antonio Navarra, Joe Tribbia, Stefan Klus, and Paula Lorenzo-Sánchez. Variability of sst through koopman modes. *Journal of Climate*, 37(16):4095–4114, 2024.

[19] Yann Ollivier, Hervé Pajot, and Cédric Villani. *Optimal transport: theory and applications*, volume 413. Cambridge University Press, 2014.

[20] M. Raissi, P. Perdikaris, and G.E. Karniadakis. Physics-informed neural networks: A deep learning framework for solving forward and inverse problems involving nonlinear partial differential equations. *Journal of Computational Physics*, 378:686–707, 2019.

[21] Huanfeng Shen, Xinghua Li, Qing Cheng, Chao Zeng, Gang Yang, Huifang Li, and Liangpei Zhang. Missing information reconstruction of remote sensing data: A technical review. *IEEE Geoscience and Remote Sensing Magazine*, 3(3):61–85, 2015.

[22] Utkarsh Utkarsh, Pengfei Cai, Alan Edelman, Rafael Gomez-Bombarelli, and Christopher Vincent Rackauckas. Physics-constrained flow matching: Sampling generative models with hard constraints. *arXiv preprint arXiv:2506.04171*, 2025.

[23] Wei Xiong, Xiaomeng Huang, Ziyang Zhang, Ruixuan Deng, Pei Sun, and Yang Tian. Koopman neural operator as a mesh-free solver of non-linear partial differential equations. *Journal of Computational Physics*, 513:113194, September 2024.

Appendix

A Detailed derivation of proposed methodology

A.1 Variational inference framework

A.1.1 Probabilistic modeling

We model the physical constraint embedding mapping $H : \mathcal{Z} \to \mathcal{Y}$ as a random function in the reproducing kernel Hilbert space $\mathcal{H}_k$.

Prior distribution definition:

$$p(H) = \mathcal{GP}(0, k(z, z')) \cdot \exp\left(-\lambda \int_{\mathcal{Z}} \|F(H(z))\|^2 d\mu(z)\right)$$

Where:

- $k(z, z')$ is the kernel function, common choices include RBF kernel: $k(z, z') = \exp(-\|z - z'\|^2/2\sigma^2)$
- $F(\cdot)$ is the physical constraint function
- $\mu(z)$ is the measure on the input space
- $\lambda > 0$ is the constraint strength parameter

Likelihood function:

$$p(y|H, z) = \mathcal{N}(y; H(z), \sigma^2 I)$$

Posterior distribution: According to Bayes' theorem:

$$p(H|D) = \frac{p(D|H)p(H)}{p(D)} \propto p(D|H)p(H)$$

Where the observed data $D = \{(z_i, y_i)\}_{i=1}^N$.

A.1.2 Variational approximation

Since the true posterior distribution is difficult to calculate, we use the variational distribution $q_\phi(H)$ for approximation:

$$q_\phi(H) = \mathcal{GP}(\mu_\phi(z), k_\phi(z, z'))$$

Where $\phi = \{\mu_\phi, k_\phi\}$ is the variational parameter.

Derivation of variational lower bound (ELBO):

$$\log p(D) = \mathbb{E}_{q_\phi(H)}[\log p(D)] \geq \mathbb{E}_{q_\phi(H)}[\log p(D|H)] - \mathrm{KL}(q_\phi(H)\|p(H))$$

Data fitting term:

$$\mathbb{E}_{q_\phi(H)}[\log p(D|H)] = -\frac{1}{2\sigma^2}\sum_{i=1}^{N}\mathbb{E}_{q_\phi(H)}[\|y_i - H(z_i)\|^2] - \frac{N}{2}\log(2\pi\sigma^2)$$

Using the regenerative property of RKHS:

$$\mathbb{E}_{q_\phi(H)}[H(z)] = \mu_\phi(z)$$

$$Var_{q_\phi(H)}[H(z)] = k_\phi(z,z)$$

Therefore:

$$\mathbb{E}_{q_\phi(H)}[\|y_i - H(z_i)\|^2] = \|y_i - \mu_\phi(z_i)\|^2 + k_\phi(z_i,z_i)$$

KL divergence term: For the KL divergence between two Gaussian processes:

$$\mathrm{KL}(q_\phi(H)\|p(H)) = \frac{1}{2}\left[\mathrm{tr}(K_p^{-1}K_q) - \log\frac{|K_q|}{|K_p|} + \mu_\phi^T K_p^{-1}\mu_\phi - d\right]$$

Where K_p, K_q are the covariance matrices corresponding to the prior and variational distributions, respectively, and d is the dimension.

A.2 Optimal transport constraint

A.2.1 Definition of constraint violation measure

Push-forward operator: For mapping H and constraint function F, define push-forward operator:

$$(F \circ H)_{\#}\mu_Z(A) = \mu_Z(\{z \in \mathcal{Z} : F(H(z)) \in A\})$$

Constraint violation measure:

$$\nu_H = (F \circ H)_{\#}\mu_Z$$

This measure describes the distribution of constraint violation values $F(H(z))$.

Target measure:

$$\nu_0 = \delta_0$$

That is, the Dirac measure at the origin of the constraint space, indicating the situation where the constraints are perfectly satisfied.

A.2.2 Wasserstein distance calculation

2-Wasserstein distance definition:

$$W_2^2(\nu_H, \nu_0) = \inf_{\gamma \in \Pi(\nu_H, \nu_0)} \int_{\mathbb{R}^m \times \mathbb{R}^m} \|x - y\|^2 d\gamma(x, y)$$

Where $\Pi(\nu_H, \nu_0)$ is the joint distribution set with marginal distributions of ν_H and ν_0.

For the target measure $\nu_0 = \delta_0$:

$$W_2^2(\nu_H, \delta_0) = \int_{\mathbb{R}^m} \|x\|^2 d\nu_H(x) = \mathbb{E}_{z \sim \mu_Z}[\|F(H(z))\|^2]$$

Entropy regularization: To improve numerical stability, entropy regularization is introduced:

$$W_{2,\epsilon}^2(\nu_H, \nu_0) = \inf_{\gamma \in \Pi(\nu_H, \nu_0)} \left\{ \int \|x - y\|^2 d\gamma(x, y) + \epsilon H(\gamma) \right\}$$

Where $H(\gamma) = -\int \log \frac{d\gamma}{d(\nu_H \otimes \nu_0)} d\gamma$ is the relative entropy.

A.2.3 Sinkhorn algorithm implementation

Discretization approximation: For the sampling point $\{z_j\}_{j=1}^{N_s}$, the empirical approximation of the constraint violation measure is:

$$\hat{\nu}_H = \frac{1}{N_s} \sum_{j=1}^{N_s} \delta_{F(H(z_j))}$$

Cost matrix:

$$C_{ij} = \|F(H(z_i)) - 0\|^2 = \|F(H(z_i))\|^2$$

Sinkhorn iteration:

1. Initialization: $u^{(0)} = \mathbf{1}_{N_s}, v^{(0)} = \mathbf{1}_1$
2. Calculate the kernel matrix: $K_{ij} = \exp(-C_{ij}/\epsilon)$
3. Iterative update:
   - $u^{(k+1)} = \frac{1}{Kv^{(k)}}$
   - $v^{(k+1)} = \frac{1}{K^T u^{(k+1)}}$
4. Convergence judgment: $\|u^{(k+1)} - u^{(k)}\|_\infty < \text{tol}$

Optimal transmission plan:

$$P_{ij}^* = u_i^* K_{ij} v_j^*$$

Optimal transmission cost:

$$W_{2,\epsilon}^2(\hat{\nu}_H, \nu_0) = \langle P^*, C \rangle = \sum_{i,j} P_{ij}^* C_{ij}$$

A.3 Complete optimization algorithm

A.3.1 Overall loss function

Variational lower bound:

$$\mathcal{L}_{ELBO}(\phi) = -\frac{1}{2\sigma^2}\sum_{i=1}^{N}[\|y_i - \mu_\phi(z_i)\|^2 + k_\phi(z_i, z_i)] - \frac{1}{2}\mathrm{KL}(q_\phi(H)\|p(H))$$

Constraint term:

$$\mathcal{L}_{constraint}(\phi) = \mathbb{E}_{q_\phi(H)}[W^2_{2,\epsilon}(\nu_H, \nu_0)]$$

Total loss:

$$\mathcal{L}_{total}(\phi) = \mathcal{L}_{ELBO}(\phi) + \gamma\mathcal{L}_{constraint}(\phi)$$

A.3.2 Gradient calculation

Gradient about variational parameters:

For mean function parameters:

$$\frac{\partial\mathcal{L}_{ELBO}}{\partial\mu_\phi} = \frac{1}{\sigma^2}\sum_{i=1}^{N}(y_i - \mu_\phi(z_i)) + K_p^{-1}\mu_\phi$$

For covariance parameters:

$$\frac{\partial\mathcal{L}_{ELBO}}{\partial k_\phi} = -\frac{1}{2\sigma^2}\mathbf{1} + \frac{1}{2}(K_p^{-1} - K_q^{-1})$$

Constraint gradient (back-propagation through Sinkhorn algorithm):

$$\frac{\partial\mathcal{L}_{constraint}}{\partial\phi} = \frac{\partial W^2_{2,\epsilon}}{\partial F(H)}\frac{\partial F(H)}{\partial H}\frac{\partial H}{\partial\phi}$$

B Preliminary experimental verification

B.1 Experimental setup

B.1.1 Dataset construction

This preliminary experiment uses the one-dimensional heat conduction equation as a verification case:

$$\frac{\partial u}{\partial t} = \alpha\frac{\partial^2 u}{\partial x^2} \tag{1}$$

The experimental data is generated by the Crank-Nicolson implicit difference method, and the specific parameters are set as follows:

- Number of spatial discrete points: $n_x = 100$
- Spatial domain length: $L = 1.0$, that is, $x \in [0, 1]$
- Total simulation time: $T = 1.0$
- Time step: $dt = 0.001$
- Thermal diffusion coefficient: $\alpha = 0.01$
- Noise level: noise_level = 0.01
- Spatial step: $dx = L/(n_x - 1) \approx 0.0101$
- Time step: $n_t = 1001$, save interval is 10 steps

The data set contains four different types of initial conditions:

- **Gaussian pulse**: $u_0(x) = \exp(-(x - x_c)^2/\sigma^2)$
- **Sine wave**: $u_0(x) = \sin(n\pi x)$
- **Step function**: $u_0(x) = H(x - x_c)$
- **Random Fourier combination**: $u_0(x) = \sum_k a_k \sin(k\pi x) + b_k \cos(k\pi x)$

The final dataset size is: 1000 cases for training set, 200 cases for validation set, and 200 cases for test set. Each sample contains 100 time slices, and each slice has 100 temperature values at spatial locations.

B.1.2 Model architecture

The experiment adopts a simplified Koopman autoencoder architecture, the specific structure is as follows:

Encoder ($\phi_{NN} : \mathbb{R}^{100} \to \mathbb{R}^{32}$):

- Input layer: $100 \to 64$ (BatchNorm + ReLU + Dropout(0.1))
- Hidden layer 1: $64 \to 128$ (BatchNorm + ReLU + Dropout(0.1))
- Hidden layer 2: $128 \to 256$ (BatchNorm + ReLU + Dropout(0.1))
- Output layer: $256 \to 32$ (Linear layer)

Koopman operator ($\phi_K : \mathbb{R}^{32} \to \mathbb{R}^{32}$):

- Linear transformation: $K \in \mathbb{R}^{32\times32}$ (no bias)

decoder ($H : \mathbb{R}^{32} \to \mathbb{R}^{100}$):

- The structure is symmetrical with the encoder, and the dimension decreases layer by layer

B.1.3 Training configuration

- **Number of training rounds**: 100 epochs
- **Optimizer**: Adam, initial learning rate 0.001
- **Learning rate schedule**: StepLR, decay factor $\gamma = 0.97$, decay every 50 rounds
- **Loss function weight**:

$$\mathcal{L}_{total} = w_{recon}\mathcal{L}_{recon} + w_{pred}\mathcal{L}_{pred} + w_{phys}\mathcal{L}_{phys} + w_{lin}\mathcal{L}_{lin} \tag{2}$$

$$= 1.0 \cdot \mathcal{L}_{recon} + 1.0 \cdot \mathcal{L}_{pred} + 0.1 \cdot \mathcal{L}_{phys} + 0.01 \cdot \mathcal{L}_{lin} \tag{3}$$

B.2 Experimental results analysis

B.2.1 Error distribution characteristics

Error distribution analysis (Figure 2 (a)) shows the following key features:

- **Right-skewed distribution**: All error types (reconstruction, 1-step prediction, 5-step prediction, 10-step prediction) show right-skewed distribution. This means that most predictions are quite accurate, but a small number of samples have noticeably larger errors.
- **Multi-step prediction stability**: Importantly, multi-step prediction errors do not show significant growth over time. This supports the assumption that Koopman dynamics remain stable over short horizons under the current setup.

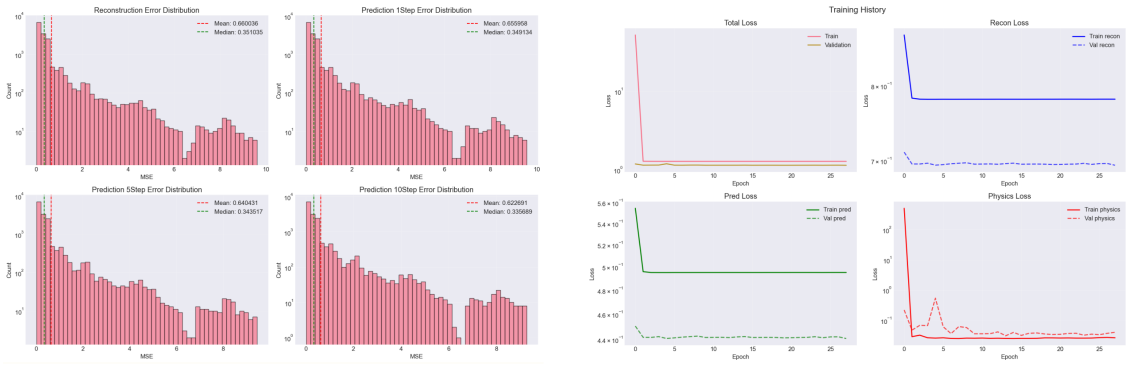

(a) Error distribution statistics chart

(b) Training process loss curves

Figure 2: (a) Shows the error statistics graph of the trained model for predictions at different time steps. (b) Shows the convergence of different loss curves on the training set and validation set during training.

B.2.2 Convergence of training process

The training process (Figure 2 (b)) shows good convergence characteristics:

- **Stable convergence**: All loss terms converge smoothly without obvious overfitting.
- **Physical constraint effectiveness**: The physical loss term drops sharply, confirming that the L_2 regularization helps enforce physical consistency during training.
- **Target balance**: The prediction loss remains stable, indicating that adding physical constraints does not threaten the main prediction performance of the model.
- **Early convergence**: The model reaches its best performance by around the 28th epoch, hinting at the limited capacity of the current architecture to further improve.

B.2.3 Analysis of latent space representations

Correlation between dimensions: The 32-dimensional representations of the latent space (Figure 3 (a)) show obvious structural block correlation patterns, and there are also some strong negative correlations, which indicates that:

- The encoder appears to capture meaningful cluster-like patterns.

- Physical constraints seem to encourage a more structured latent space.
- Some dimensions show redundancy, suggesting that future versions could benefit from reducing the latent dimensionality.

Dynamic trajectory features: The latent space trajectory after PCA dimensionality reduction (Figure 3 (b)) shows approximately piecewise linear features, and the trajectory is stable without obvious ring or winding structure, which strongly supports the effectiveness of Koopman's linear evolution hypothesis in the latent space.

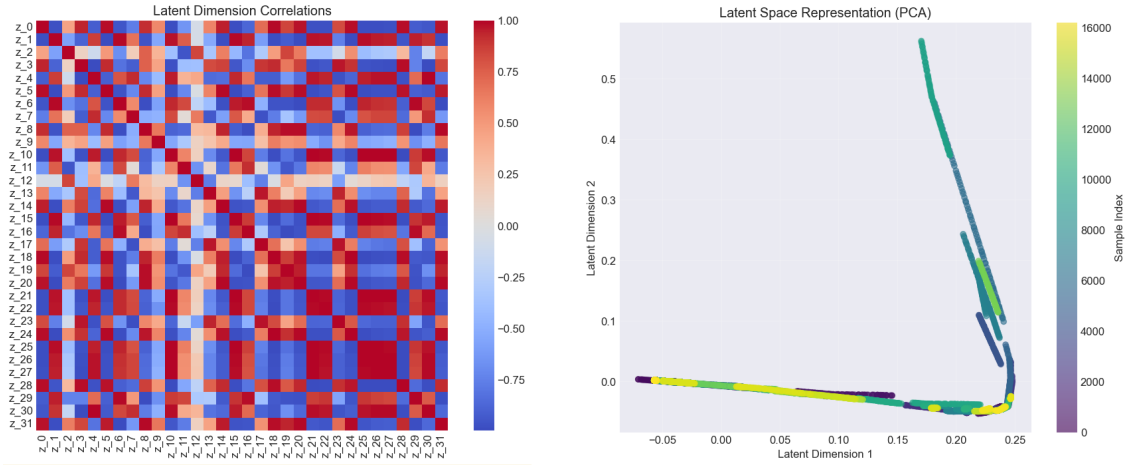

(a) Hidden space variable correlation map

(b) Hidden Space PCA Visualization

Figure 3: (a) Displays the correlation diagram of each variable in the latent space. (b) Presents the distribution of the latent space after dimension reduction using PCA.

B.2.4 Prediction quality evaluation

Visual results (Figure 4) show:

- **Spatial error distribution**: Most prediction errors occur near the domain boundaries, while the central regions are predicted with high accuracy.
- **Time evolution stability**: The model stably maintains the main trend of heat diffusion during the multi-step evolution process.
- **No systematic deviation**: There is no obvious systematic pattern in the error distribution, indicating that the model successfully captures the global physical behavior.

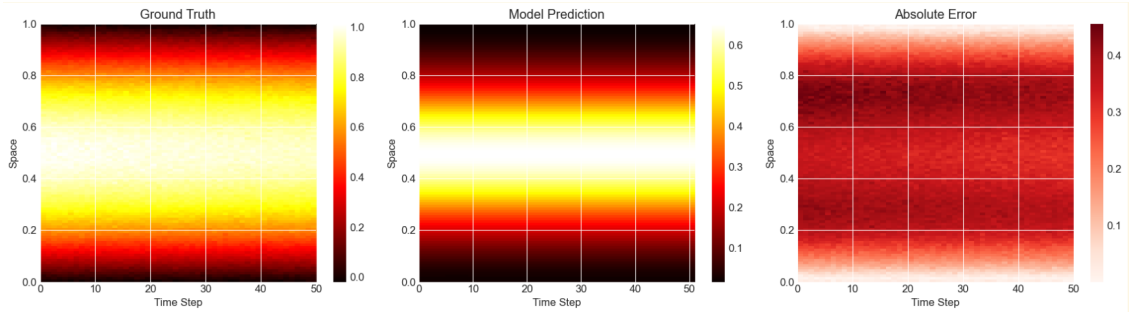

Figure 4: Use the trained simplified model to perform autoregressive inference on a test set sample.

For more detailed analysis, please refer to my test framework at Github

B.3 Preliminary conclusions and findings

B.3.1 Method validity verification

Early experiments suggest that the proposed framework is fundamentally sound:

- **Koopman structure preservation**: Even with a simplified setup, the model maintains the core linear dynamics expected from the Koopman framework.
- **Physical constraint integration**: The use of soft physical constraints during training helps embed prior knowledge into the model and improves performance.

B.3.2 Limitations and further improvements

At the same time, the experiments highlight several areas that need further attention:

- **Limited expressiveness**: The use of a purely linear architecture may restrict the model's ability to capture finer spatial features.
- **Boundary error**: Errors near the domain boundaries remain significant, indicating the need for more effective boundary handling strategies.
- **Scalability**: The effectiveness of the method needs to be further verified on higher-dimensional and more complex systems.

This preliminary experiment has laid a solid foundation for subsequent verification on complex systems and proved the feasibility and potential of the core methodology.